Materials Today Communications 38 (2024) 107868

Contents lists available at ScienceDirect

Materials Today Communications

journal homepage: www.elsevier.com/locate/mtcomm

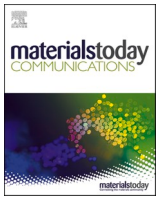

TEM morphological analysis of biopolymers: The case of Poly (Lactic Acid) (PLA)

Giovanna Molinari [a,b], Paola Parlanti [b], Laura Aliotta [a,c], Andrea Lazzeri [a,c], Mauro Gemmi [b,*]

[a] Department of Civil and Industrial Engineering, University of Pisa, 56122 Pisa, Italy
[b] Electron Crystallography, Center for Materials Interfaces, Istituto Italiano di Tecnologia, 56025 Pontedera, Italy
[c] National Interuniversity Consortium of Materials Science and Technology (INSTM), 50121 Florence, Italy

ARTICLE INFO

Keywords:
Polymer staining
Crystalline structure
Spherulite
Sectioning
TEM imaging
Poly (lactic acid) (PLA)
Biopolymers

ABSTRACT

Transmission Electron Microscopy (TEM) is one of several techniques for studying the morphology of polymers, which allows the analysis of their micro- and nano-domains, providing essential insights into their fundamental properties. To achieve such information, this paper proposes an extensive TEM characterisation of a crystalline Poly (Lactic Acid) (PLA), one of the first fully biobased and biodegradable polymers able to compete with traditional polymers in terms of performance. Further, the investigated biopolymer will be manufactured by injection moulding, one of the main industrial processing techniques in the field of biopolymer production. To improve TEM imaging, the best staining/coating conditions of PLA thin sections will be determined. Then, it will be described the arrangements of spherulites in PLA, as well as their lamellar organization within, by exploiting different sample sectioning approaches (i.e., directional and serial).

1. Introduction

Polymers are among the most revolutionary materials in the contemporary world [1]. Indeed, thanks to the wide range of features that they exhibit (high strength, lightweight, toughness, corrosion resistance, transparency, good processability, and low cost [2]), people use them in every daily life. Synthetic polymers, though, pose several issues related to the conflicting nature of their durability and degradability properties.

For most applications, it is ideal for the material to retain certain properties over time, but it is also desirable for it to be easily disposable after use. Indeed, a huge amount of material ends up in landfills or even abandoned, and some of it ends up in the sea [3]: a waste management that has become a crisis due to limited landfill capacity, high costs and environmental pollution problems [4]. For this reason, it is necessary to find an alternative that can facilitate the end-use processes from both a financial and environmental point of view [5].

A relevant technological innovation, based on the rediscovery of the latent value of renewable bio-resources and sustainable production as a new development paradigm, lies in the concepts of “bioeconomy” and “bio-circularity”. From this perspective, the new class of biobased and biodegradable polymers is likely to contribute for the global transition to a circular and post-carbon world, which aims to replace the more conventional petrochemical-derived plastics [6,7].

Poly (lactic acid) (PLA), a biobased and biodegradable polyester, is widely used in a variety of daily-use products thanks to its ability to be easily processed by using traditional manufacturing techniques such as injection moulding, blow moulding, cast extrusion, and thermoforming, as well as to its good mechanical properties [8]. PLA is generally regarded as one of the top bioplastics due to its renewable origin, versatility, lower greenhouse gas emissions, and reduced dependence on petroleum [9].

Compared with other common bioplastics (such as polyhydroxybutyrate [10], polyhydroxyalkanoates [11], polycaprolactone [12]), PLA has wider applications, both for disposable and durable products (packaging materials, disposable cutlery, textiles, medical implants, 3D printing filaments) [13]. It also exhibits properties that can be tailored through modifications of its chemical structure, such as copolymerization with other monomers or the addition of additives, in order to improve its heat resistance, flexibility or impact resistance [14]. A series of characteristics that makes PLA a versatile bioplastic and increases its presence on the market compared to other bioplastics (PHA, etc.).

Thus, it is essential to study PLA inherent properties (mechanical,

* Corresponding author.
E-mail addresses: giovanna.molinari@phd.unipi.it, giovanna.molinari@iit.it (G. Molinari), paola.parlanti@iit.it (P. Parlanti), laura.aliotta@unipi.it (L. Aliotta), andrea.lazzeri@unipi.it (A. Lazzeri), mauro.gemmi@iit.it (M. Gemmi).

https://doi.org/10.1016/j.mtcomm.2023.107868
Received 23 August 2023; Received in revised form 22 November 2023; Accepted 13 December 2023
Available online 18 December 2023

chemical, and thermal), which are directly and closely related to its structural and morphological characteristics, to take a first step towards the development of environmental friendly polymeric materials with desired properties [15]. Indeed, the selection of the "best" bioplastic is contingent on specific application and environmental considerations.

Since 1990, morphological investigations of polymeric materials are conducted by using a variety of microscopy techniques: among those, scanning electron microscopy (SEM) and atomic force microscopy (AFM) provide accurate information of the polymers morphology with nanometric resolution [16,17]. Nevertheless, the typical polymeric structural disorder and polydispersity, associated with the amorphous-phase component, are parameters that may render challenging the data interpretation [18].

Transmission Electron Microscopy (TEM) allows the investigation of morphological details concealed in tiny domains. Since the repetition scales in polymer morphologies are of the same order as the dimensions of the molecular details (few nanometres), TEM imaging represents an invaluable characterisation tool in polymer science [19]. However, polymers preparation for TEM characterization is challenging. Indeed, polymeric materials are constituted by only light elements (C, H, O, and others), which weakly interact with the electron beam; thus, the contrast between structural details is very low. Also, TEM analysis can be only performed on thin samples (few hundred nanometres thick): polymers should be sectioned by means of an ultramicrotome to obtain thin slices [20]. Finally, polymers are beam-sensitive materials, which commonly are subjected to their damage [17] during electron microscopy analysis [21,22]. For instance, PLA has a degree of degradation which is strongly influenced by radiation (caused by the existence of catalyst remnants like hydro peroxide and carbonyl groups) and/or water. So, once the polymer is exposed to radiation, the primary chain scission happens, resulting in mechanical deterioration that also may facilitates its microbial and oxidative degradation [23,24]. Therefore, reducing the electron dose [19,25–27], as well as operating in cryogenic conditions [28], would decrease the loss of volatile components from the sample, while minimizing its damage due to the electron beam [29]. Indeed, at low temperatures the mobility of polymer molecules and all secondary processes (e.g., mass loss, crystal amorphization rate, cross-linking) are reduced [30,31]. Likewise, chemical staining obtained through the incorporation of heavy elements (e.g., osmium tetroxide, ruthenium tetroxide, phosphoric acid-tungsten, etc. [18]) can be employed to address the low-contrast issue, thereby allowing different structural details to be evidenced [32].

The aim of this study will be the performing a TEM morphological characterization of the crystalline structure of an injection-moulded PLA. The injection moulding technique is, here, adopted as it is one of the most widely employed in plastics industry [33]. This would provide useful information about the orientation and size of the crystalline domains, as well as the presence of any potential morphological defects such as voids, inclusions, or phase separations within the polymer. In addition, new insights would be gained into the amorphous and semicrystalline phase of the system: microscopical features directly related to the material properties, such as transparency, flexibility, stiffness, strength, and thermal behaviour.

According to Ye et al. [34], highly oriented crystalline domains may lead to increased tensile strength, material stiffness, melting point [35] and higher thermal conductivity [36] compared with more amorphous polymeric systems. Moreover, Murmu and coworkers [37] point out that smaller crystalline domains could result in both elasticity decrease [38] and increased toughness, as they could act as barriers to crack initiation and propagation. Also, as shown by Lin et al. [39], smaller and less organized domains decrease the opacity and translucency of the polymer.

Improvements in the thermal (higher heat resistance [43]) and mechanical-rheological (increased loss/storage ratio [44]) properties of PLA are detectable within the crystallization temperature range of 100–120 °C [43], therefore most of the industrial processing are carried out in this temperature range [40–42]. For this reason, the morphology and the crystallization kinetics of PLA treated at T = 110 °C will be characterized in this study. Several staining protocols will be evaluated for PLA sections to be characterized by TEM, to define the one that overcomes the issues related to contrast and beam damage. Relying on two different approaches for ultramicrotome sectioning ("directional" and "serial sectioning"), an extensive description of the PLA morphology will be carried out. Finally, the type of PLA constituent crystalline structures (i.e., spherulites), their architecture and spatial arrangement and the three-dimensional reconstruction of a single spherulite will be described in detail.

2. Materials and methods

2.1. Materials

Commercial PLA Ingeo 3100HP (here named PLA) derived from natural resources was purchased from NatureWorks LLC. According to the producer datasheet, this PLA-grade contains about 0.3% of D-lactic acid units [MFR: 24 g/10 min (210 °C, 2.16 kg); nominal average molar mass: 120,000 g/mol; density: 1.24 g/cm^3].

2.2. Injection moulding

Before the injection moulding, the PLA granules were dried in a DP604–615 PIOVAN dryer (Venezia, Italy) at 60 °C for 24 h. The injection moulding was carried out on a Megatech H10/18 injection moulding machine (TECNICA DUEBI S.r.l. Fabriano, Italy), to obtain ISO 527–1 A dog-bone specimens (width: 10 mm, thickness: 4 mm, length: 80 mm). The semicrystalline PLA-specimens were prepared by varying the moulding time (t_{mould}), according to the performed isothermal crystallization measurements. The temperature screw profile adopted for the injection moulding was: 185/190/185/180 °C from the hopper to the die, the mould was set at 110 °C and the injection pressure at 90 bar. The injection moulded PLA specimens were placed in a dry keeper (SANPLATEC Corp. (Osaka, Japan)) at room temperature and 50% humidity for 3 days before further characterizations.

2.3. Thermal analysis

Differential scanning calorimetry (DSC) analysis was performed on a DSC Q200 TA-Instrument (New Castle, UK) equipped with a radiative sky cooling system (RSC). For all measurements, nitrogen was adopted as purge gas (set at 50 mL/min). The instrument was calibrated with indium, used as standard for temperature and enthalpy calibrations. The materials used for DSC were cut from the injection moulded specimens. About 10–15 mg of were sealed inside aluminium hermetic pans and each sample was tested only once.

The following thermal program was adopted: equilibrate the sample at 25 °C for 2 min, heating ramp up to 190 °C at 20 °C/min followed by an isothermal step at 190 °C for 2 min. To estimate the PLA isothermal crystallization behaviour, the sample was cooled at 100 °C/min down to 110 °C and held for 30 min. Finally, it was heated at 10 °C/min to 190 °C and held for 2 min to record the crystallization and melting behaviours. The melting temperature (T_m) of the specimen was determined by considering the maximum of the melting peaks. The melting enthalpy was determined from the corresponding peak areas in the thermograms. The crystallinity percentage of PLA was calculated according to the equation Eq. 1 [45,46]:

$$\chi = \frac{(\Delta H_m - \Delta H_c)}{\Delta H^0{}_m \bullet X_{PLA}} \quad (1)$$

where ΔH_m and ΔH_c are the PLA melting and cold crystallization enthalpies calculated as the integral of the areas underlain by two curves, respectively; X_{PLA} is the PLA weight fraction in the formulation and ΔH^0_m

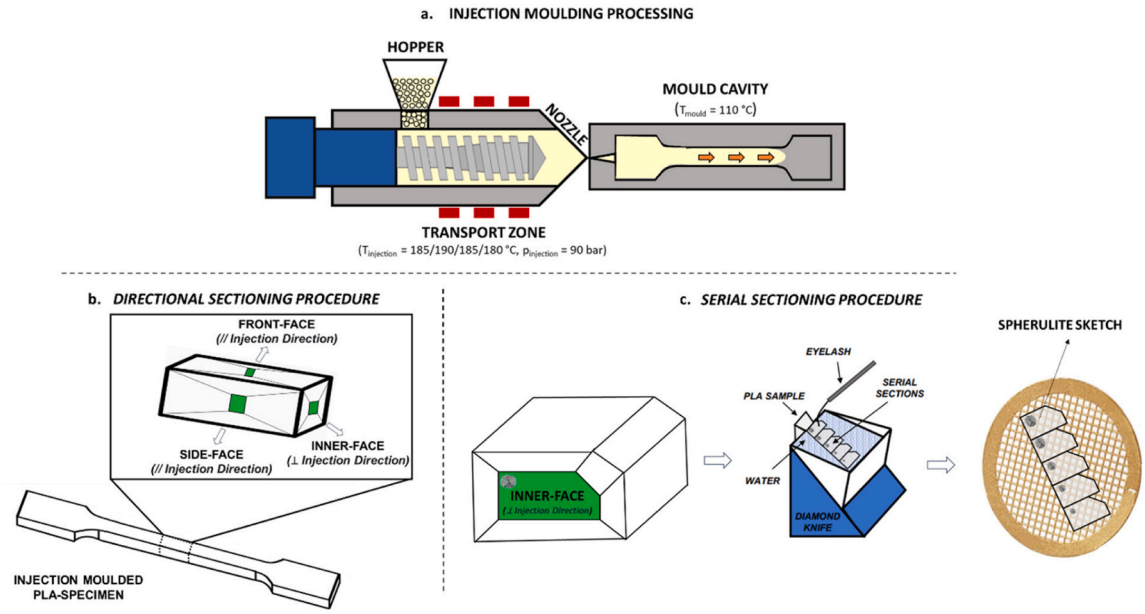

Fig. 1. **a.** Schematization of the injection moulding processing, where orange arrows indicate the injection direction of the polymeric melt within the hot-mould. **b.** Directional sectioning. **c.** Serial sectioning.

is the melting enthalpy (equal to 93 J/g [47]) of the 100% crystalline PLA.

2.4. X-ray diffraction (XRD) analysis

XRD data were acquired with transmission/Debye-Scherrer geometry using a STOE Stadi P diffractometer equipped with Cu-Kα_1 radiation ($\lambda = 1.5406$ Å), a Ge (1 1 1), a Johansson monochromator from STOE & Cie and a MYTHEN2 1 K detector from Dectris. The line focused Cu X-ray tube was operated at 40 kV and 40 mA. Data were acquired in the 2θ range 2–60° (maximum resolution ca. 1.5 Å) with an interval of 0.03° between consecutive points. A scan without samples was performed and appropriately scaled for each scan, to avoid the air scattering contribution. The X-ray crystalline fractions (X_C^{XRD}) were calculated as the ratio of the areas of the crystalline peaks to the total area of the background corrected diffraction profile. The lattice constants were calculated from the positions of the most XRD intense peaks ascribable to the PLA α-form.

2.5. Sectioning

Small PLA blocks (approx. 5 mm sides) were obtained from the injection moulded PLA samples by using a jigsaw. Blocks were mounted on an ultramicrotome (UC7, Leica Microsystem, Vienna, Austria), trimmed with a razor blade to reduce the block size down to 1 mm sides, and PLA block faces were polished by using home-made glass knives (EM KMR3, Leica Microsystem). Finally, the blocks were sectioned at room temperature using a 45° diamond knife (DiATOME, Nidau, Switzerland) in thick slices for light microscopy (LM) and polarized light microscopy (PLM) observations, and thin ones for TEM analysis. Sectioning was performed by keeping the ultramicrotome speed at 0.6 mm/sec.

Sections for LM and PLM (500 nm thick) were placed on a drop of distilled water placed on glass slides. The collected sections were then air dried before imaging. Thin sections for TEM imaging (90 nm thick) were placed on copper grids (either G300Cu or C-coated 300 mesh thin bar Cu grids – EMS (Hatfield, PA, USA)).

To get three-dimensional information of the sample ultrastructure, sectioning was performed with two different approaches:

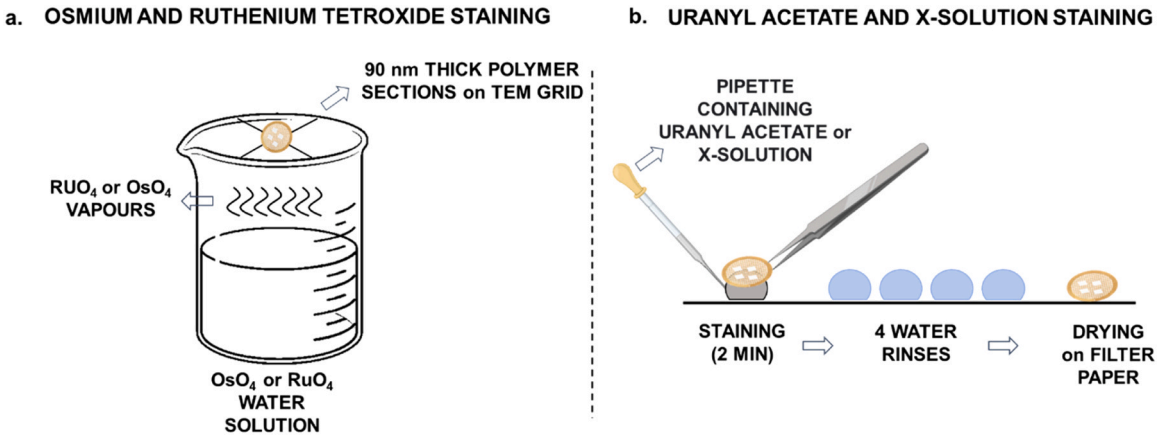

Fig. 2. Sections staining with **a.** osmium tetroxide or ruthenium tetroxide vapours and **b.** uranyl acetate or X-solution.

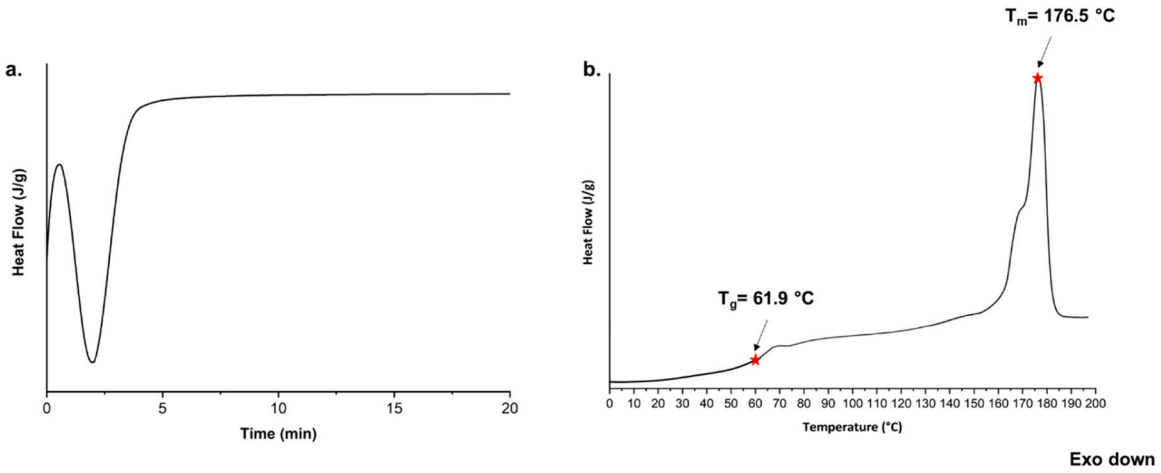

Fig. 3. a. Isothermal crystallization behaviour and **b.** melting behaviour of PLA.

- *Directional sectioning* (Fig. 1b.). The sample was ultramicrotome sectioned in three orthogonal directions with respect to the injection moulding, namely: front-face, side-face, and inner-face. During the injection moulding process, the front-face and side-face are directly in contact with the hot mould, kept at 110 °C. In contrast, the inner-face is perpendicular to the injection polymeric flow, thus it is not directly in contact with the hot mould. Sections were collected on G300Cu grids.
- *Serial sectioning* (Fig. 1c.). Several sequential thin sections of the inner-face were collected on C-coated 300-mesh thin bars Cu grids for a total thickness of few micrometres, with the aim of reconstructing, through TEM imaging of sequential sections, the entire volume of few spherulites.

2.6. Staining protocols

Four staining procedures for PLA sections placed on 300 mesh copper grids were tested:

- *Osmium Tetroxide staining and Ruthenium Tetroxide staining*. Grids with PLA thin sections were hanged on top of a beaker containing either 1% OsO_4-water solution or 1% RuO_4-water solution to expose the polymeric material to the osmium or ruthenium vapours, for 24 h at room temperature (Fig. 2a.).
- *Uranyl Acetate staining and X-solution staining*. 1.5% Uranyl Acetate water solution was adsorbed for 2 min on the polymer thin sections placed on 300 mesh copper grids. Then, grids were washed four times with distilled water (Fig. 2b.) and finally air dried. The same procedure was used to test a home-made uranyl-free staining solution (X–solution [48]), based on a pH buffered Yb^{3+}/phosphotungstic acid mixture.

2.7. Carbon coating

Unstained PLA sections placed on 300 mesh copper grids were coated with a thin film of carbon (few nanometers) to reduce charging artifacts, using an EM ACE600 (Leica Microsystems, Vienna, Austria).

Table 1
Unit Cell Parameters and X_C^{XRD} of PLA.

a [Å]	b [Å]	c [Å]	Cell Volume [Å^3]	X_C^{XRD} [%]
10.66 ± 0.05	6.03 ± 0.01	28.99 ± 0.01	1864 ± 9	32.3 ± 1.0

2.8. Optical microscopy and polarized light microscopy

500 nm thick sections were imaged with a DM750 optical microscope (Leica Microsystem, Vienna, Austria), equipped with an ICC50HD (Leica Microsystem, Vienna, Austria) digital camera. 4X HI PLAN (NA=1.59), 10X HI PLAN (NA=0.64) and 40X HI PLAN (NA=0.16) objectives (Leica Microsystem, Vienna, Austria) were used.

The same sections were also imaged using an Axio Scope A1 polarized microscope (Carl Zeiss, Oberkochen, Germany) equipped with crossed polarizers.

2.9. Transmission electron microscopy

TEM analysis was carried out using a Zeiss Libra 120 Plus transmission electron microscope, operating at 120 kV, equipped with an in-column omega filter (Carl Zeiss, Oberkichen, Germany) for energy filtered imaging, and a bottom mounted 16-bit CCD camera 2 k × 2 k (TRS).

Several low magnification images were collected for the analysis of spherulites morphology and sizes. Higher magnification images were acquired for characterizing the lamellar arrangements in the spherulites. For the volume reconstruction of a few spherulites, we collected low magnification images of the same spherulites across all the sequential sections. Then, images were aligned on top of each other and reconstructed as a volume by using ImageJ.

3. Results and discussion

3.1. Thermal analysis

The isothermal crystallization behaviour of the PLA-sample is shown in Fig. 3a. By analysing the acquired isothermal curve at 110 °C, it is possible to observe that the complete sample crystallization is reached in a time range of almost 8 min with a crystallization peak at 1.40 min and an isothermal plateau after 7 min.

By examining the exotherm curve, it is immediately noticeable that the kinetics is extremely fast. Here, the PLA under analysis has a moderate high molecular weight (M_w = 148,250 Da [49]). Long polymer chains would hamper the movement and rearrangement of polymer segments, reducing their mobility and thus making the crystallization more difficult [50]. Also, regarding nucleation, even though low-molecular-weight polymers feature fewer nucleation sites, they are more capable of forming crystalline structures at these sites. In fact, the reduced chains entanglement [51] and the lower energy barrier make the nucleation sites easily accessible to the polymer chains, as demonstrated by the work of Meinig et al. [52].

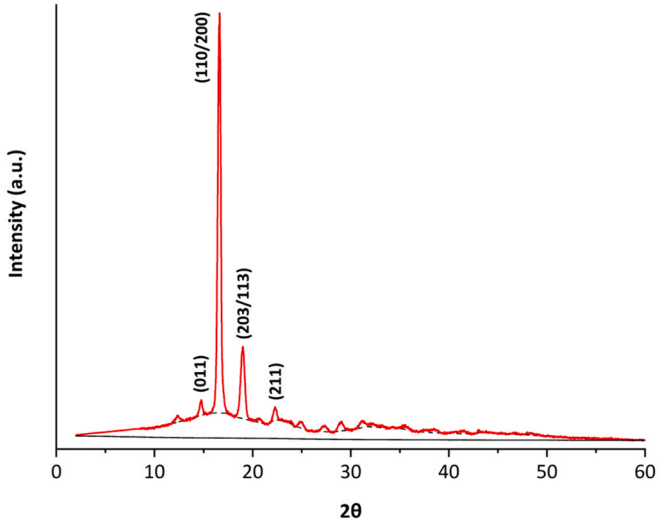

Fig. 4. XRD pattern of PLA. The scattering of the amorphous fraction (black dashed lines) and the background XRD signals (black solid line) are shown.

In the glass transition zone (Fig. 3b.), the thermogram displays a small enthalpic recovery peak or "endothermic overshoot", because of molecular relaxations that generally occur during the sample storage of 3 days at room temperature after preparation.

According to Eq. 1, the sample crystalline content, estimated from the melting endotherm, is 31.7% ($\Delta H_m = 29.5$ J/g). For comparison, the crystalline content of the sample will be also determined by XRD analysis (X_C^{XRD}) (see section below and Table 1).

Concerning the melting endotherm, it consists of two barely resolved peaks, which may be interpreted by the melting-recrystallization model [53,54]. The model assumes that the lower temperature melting endotherm is produced by the melting of the initially present lamellae that, after being partially melted, may recrystallize into structures characterized by a higher crystalline order, which would melt at higher temperatures [55]. At $T_{mould} = 110$ °C, only α-crystals grow, as also confirmed by XRD analysis (see below). Thus, the double melting behaviour can be explained as the melting of the original α-crystalline lamellae, followed by the melting of the recrystallized and more ordered α-crystals.

3.2. XRD analysis

Fig. 4 shows the XRD pattern at room temperature of PLA crystallized at 110 °C, with a mould residence time of 20 min. The XRD pattern exhibits the profile of the α-phase, identified by the position of the most intense (110/200) and (203/113) peaks at the 2θ scattering angles of 16.6° and 19.0° and by the (011) and (211) peaks at 14.7° and 22.3°, as well as for several other less intense reflections at higher angles.

It is well known that the PLA α-form is its most stable polymorph, with a left-handed 10_3 helical conformation packed in an orthorhombic unit cell [56]. Hence, according to the XRD pattern presented in Fig. 4, the average crystallographic parameters of the orthorhombic cell were calculated by combining the Bragg's law with Eq. 2 [57], using the geometrical characteristics of the (011), (200) and the (203) planes.

$$(d_{hkl})^{-2} = (h/a)^2 + (k/b)^2 + (l/c)^2 \quad (2)$$

Table 1. lists the calculated unit cell dimensions, the estimated cell volume, and the crystal fraction of the PLA-sample (X_C^{XRD}), calculated from the XRD profiles. This value is in agreement with the crystalline content estimated by means of the thermal analysis (DSC).

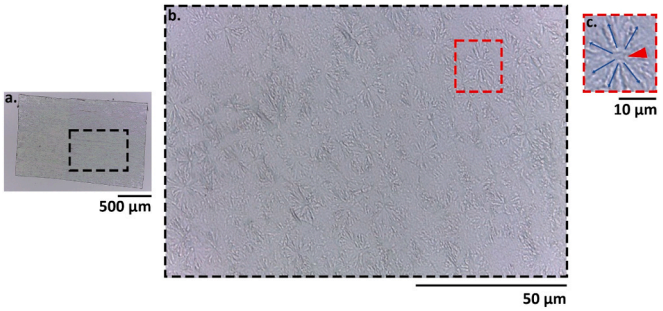

Fig. 5. a. 500 nm-thick slice image of PLA. **b.** Magnification of the area highlighted in a. One spherulite's profile is outlined with dashed line. **c.** Spherulite schematization: nucleation centre (red arrowhead), and radial branches (blue arrows).

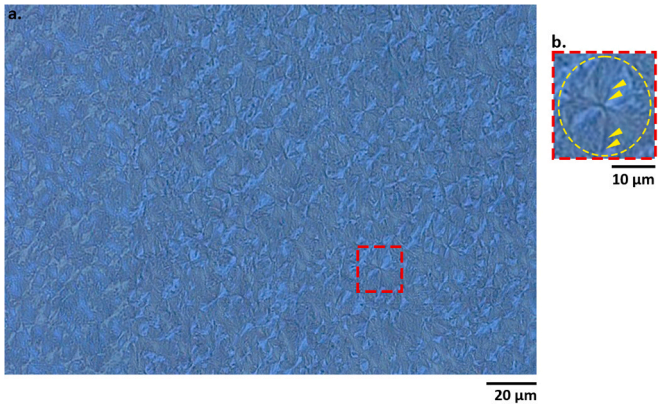

Fig. 6. a. Cross-polarized optical micrographs of a 500 nm-thick slice of PLA. **b.** A magnified spherulite from image a. highlighting the spherulitic structure (yellow ellipse). The darker coloured radial structures ascribable to PLA lamellar twisting are indicated by the yellow arrowheads.

3.3. Optical and Polarized Light Microscopy

Thick sections of PLA crystallized at 110 °C, with a mould residence time of 20 min, were placed on glass slides and firstly imaged with an optical microscope (Fig. 5). By sampling three random areas 1800 µm^2 wide, an average number of 8 ± 2 elliptical structures (i.e., spherulites), with an average area of 196.6 ± 3.1 µm^2 has been estimated.

Spherulites share a similar structure, characterized by a nucleation centre (red arrowhead in Fig. 5c.) from which radial branches (crystalline lamellae) develop (blue arrowheads in Fig. 5c.). Crystalline lamellae consist of elongated structures in the direction of the crystal growth, uniformly filling most of the available space radially outwards from a central core [58].

Fig. 6. shows cross-polarized optical micrographs of a 500 nm-thick slice of PLA. The crystal morphology (spherulites) exhibits the classical Maltese-cross extinction pattern [59,60]. If the specimen is rotated by 90° with respect to the plane of the polarized light, the two mutually orthogonal halves of the same spherulitic structure reverse their contrast indicating that the orientation of the polymer fibers/lamellae in these two regions has a strong relative rotation, as reported in the work of El-Hadi et al. [61].

Additionally, it is possible to detect some radial structures that are darker in colour than their background (yellow arrowheads in Fig. 6b.) [62]. According to Safandowska et al. [63,64], this evidence can be bound to the cooperative twisting of PLA lamellae, as it is frequently observed in lamellar structures of other polymers [61,65,66].

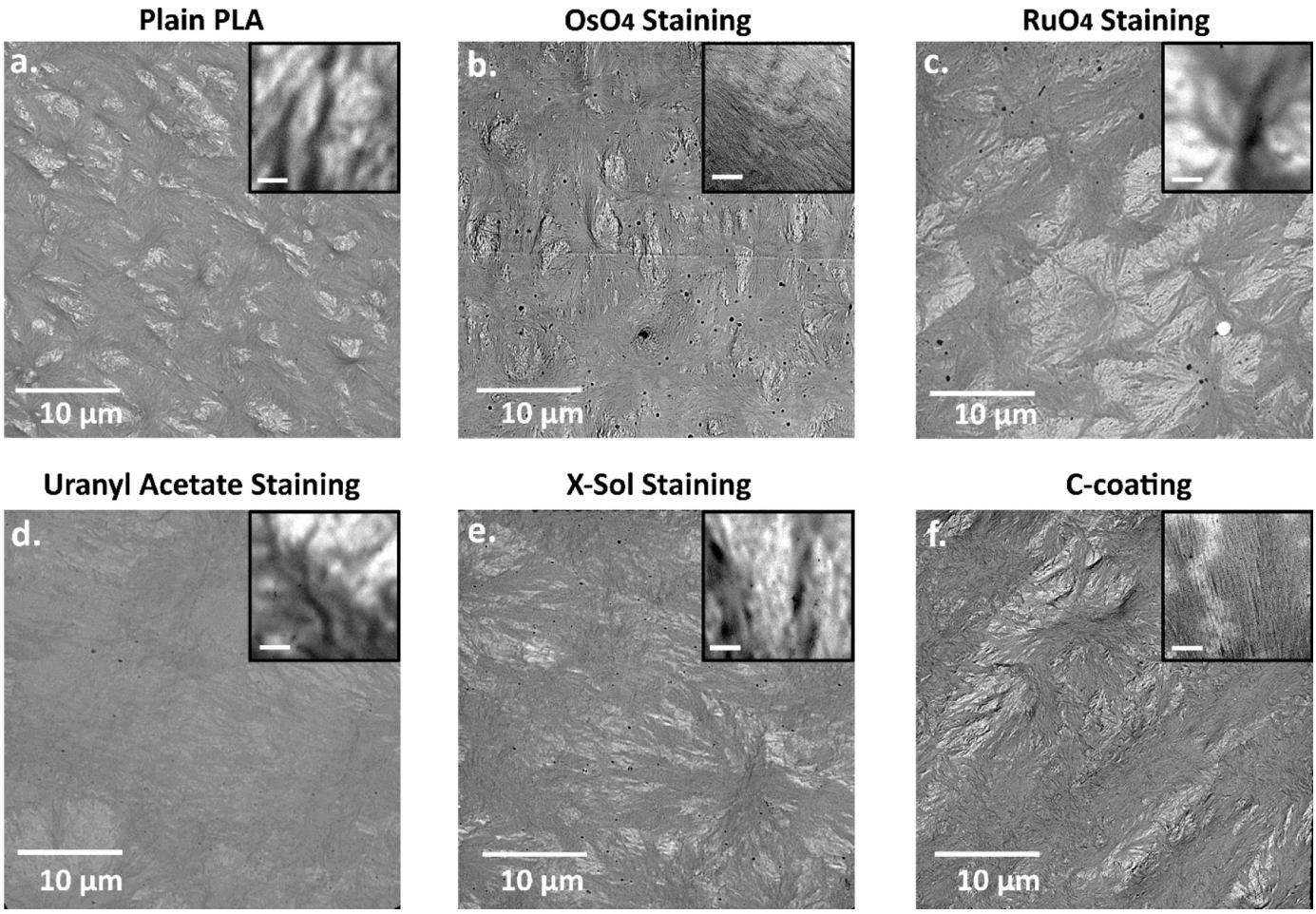

Fig. 7. Comparison of different PLA preparation procedures for TEM imaging: **a.** plain PLA section; **b.** Osmium Tetroxide staining, **c.** Ruthenium Tetroxide staining, **d.** Uranyl Acetate staining, **e.** X-solution staining and **f.** Carbon-coated PLA sections. Scalebars in the insets are 100 nm.

3.4. Preparation of Polymer Thin Sections for TEM imaging

TEM characterization of polymers usually deals with issues related to the poor contrast of the material, and its sensitivity to the electron beam. To overcome these limits, the best sample preparation method was searched by evaluating the effect of different staining protocols of PLA-sections (Fig. 7b-f.) and by comparing them with non-stained/non-coated sections (Fig. 7a.).

The staining conducted by exposing PLA sections to OsO_4 vapours for 24 h reveals spherulitic shapes with internal radial lamellar arrangements (Fig. 7b. and inset). RuO_4 stained sections (Fig. 7c.) retain the same characteristics showing well defined spherulites boundaries. However, at higher magnification, the typical lamellar arrangements cannot be visualized.

On the other hand, the use of Uranyl Acetate staining solution appears to mitigate the contrast enhancement effect provided by the OsO_4/RuO_4-staining (Fig. 7d.), even though some morphological features are still visible in specific areas. In addition, at higher magnification, the images are blurred. Similar results were observed on X-solution stained sections (Fig. 7e.). This difference compared with OsO_4/RuO_4 staining may be directly related to the sensitivity of PLA to water exposure. Indeed, it is well-known that water leads to PLA intrinsic hydrolytic degradation, through random cleavage mechanisms of its ester bonds in a heterogeneous and autocatalytic fashion [14,67]. This evidence could explain the weak contrast of sections stained by placing them on water solution drops (Uranyl Acetate or X-solution), as illustrated in Fig. 2b.

Remarkably, carbon coating is discovered to improve the spherulites contrast, while also allowing to acquire detailed higher magnification images, where lamellar details are clearly visible (Fig. 7f.), similarly to what we observed on sections exposed to OsO_4 vapours. This observation suggests that charging effects of the polymeric material is the primary issue to be faced when dealing with sample preparation for TEM imaging. If the coating/staining is not able to compensate this effect as soon as the magnification is increased, the deflection of the electron beam by the charged section perturbates the image with a consequent loss of resolution. This also suggests that the image contrast reflects an intrinsic structural feature of the spherulite, and it is not ascribable to the special coating/staining performed. Furthermore, the fact that carbon coating enhances charge dissipation while simultaneously maintaining material's naive contrast and improving TEM image quality, makes this approach a good qualifier because it also avoids the use of toxic reagents such as OsO_4.

3.5. TEM characterization of PLA

Directional sectioning was used to evaluate the development of the PLA crystalline spherulitic morphology in the three different directions of polymeric flow in the hot mould during the injection moulding, as depicted in Fig. 1a.

Szucs et. al [68] state that the orientation of the injection moulded material is often inhomogeneous, giving rise to some changes in its micro- and nanostructure. Generally, an elongational flow mainly develops in the mould centre while shearing deformation zones arise in the vicinity of the mould cavity walls. Moreover, during injection, the polymeric melt is always oriented in the direction of the flow, explaining the formation of elliptical spherulitic structures, other than

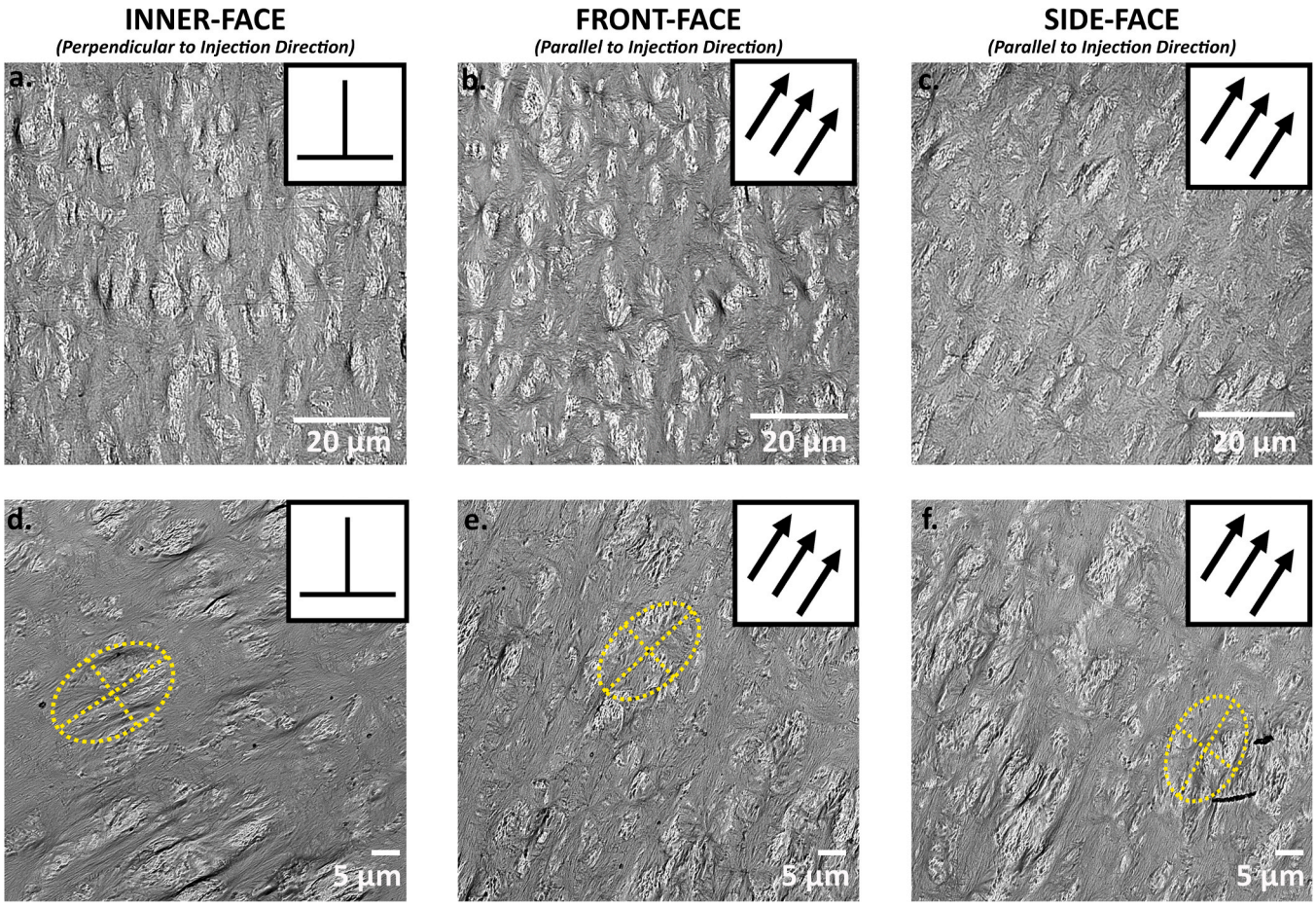

Fig. 8. Lower (top row) and higher (bottom row) magnifications TEM images of: **a,d.** inner-face, **b,e.** front-face and **c,f.** side-face sections of PLA. The direction of injection is graphically shown in the insets. Yellow dashed ellipses trace spherulites boundaries; yellow dashed lines show spherulites major and minor axis.

Table 2
TEM morphometric analysis of spherulites in directionally sectioned PLA.

Sample	Major-Axis Length [µm]	Minor-Axis Length [µm]	Area of Spherulite [µm^2]	Ellipticity
Inner-face	21.6 ± 0.6	12.2 ± 0.5	206.9 ± 2.4	0.56
Front-face	22.2 ± 1.2	11.2 ± 0.8	195.2 ± 2.1	0.50
Side-face	22.2 ± 0.9	10.7 ± 0.3	186.5 ± 1.7	0.48

spherical-like (Fig. 8b,e. (front-face) and 8c,f. (side-face)).

By sampling 30 random spherulites (10 per each sectioning direction) on TEM images, it was possible to estimate their axis lengths and areas, as well as qualitatively describe the spherulites shape for the directionally sectioned PLA (Table 2.).

During injection moulding, when the polymeric melt goes in contact with the colder mould walls, it freezes in an oriented state. Conversely, the "inner melt" is not yet fully solidified, and therefore begins to relax. This relaxation may cause the loss of spherulitic structure preferential orientation. Hence, according to the rheological evaluation of the injection moulding flow, there will be an oriented outer layer and an unoriented inner one [69–71]. In addition, Arrigo et al. [72] and Zhou et al. [73] report that crystalline structures act as nuclei for the crystallisation process and promote the growth of crystalline lamellae in a direction perpendicular to the injection one (shish-kebab structures [74, 75]). This thereby promotes their formation with a significant increase in the crystallisation kinetics of the polymer without affecting its overall crystallinity content. All these processes could explain the findings on spherulites shape of this work: spherulites at the inner face (region of the inner melt) tend to be larger and more circular compared to what detectable for spherulites at the front and side-faces. Values of ellipticity, here defined as the ratio between ellipse's minor and major-axis

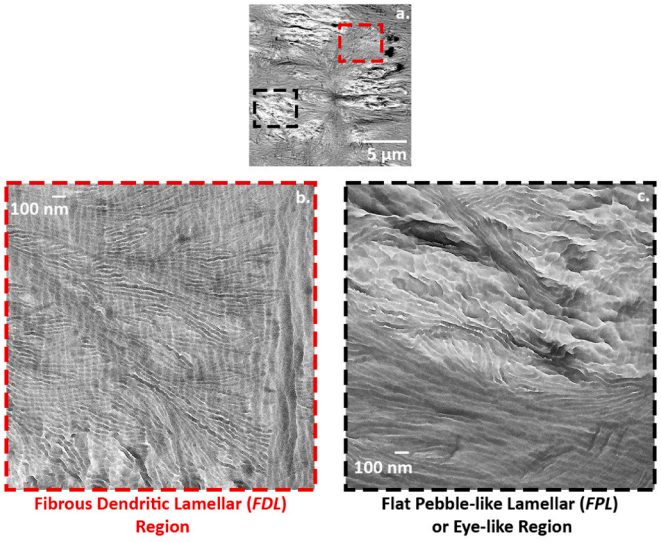

Fig. 9. a. TEM imaging of a PLA spherulitic structure (inner-face sectioned), where the **b.** FDL and **c.** FPL regions are boxed in red and black, respectively.

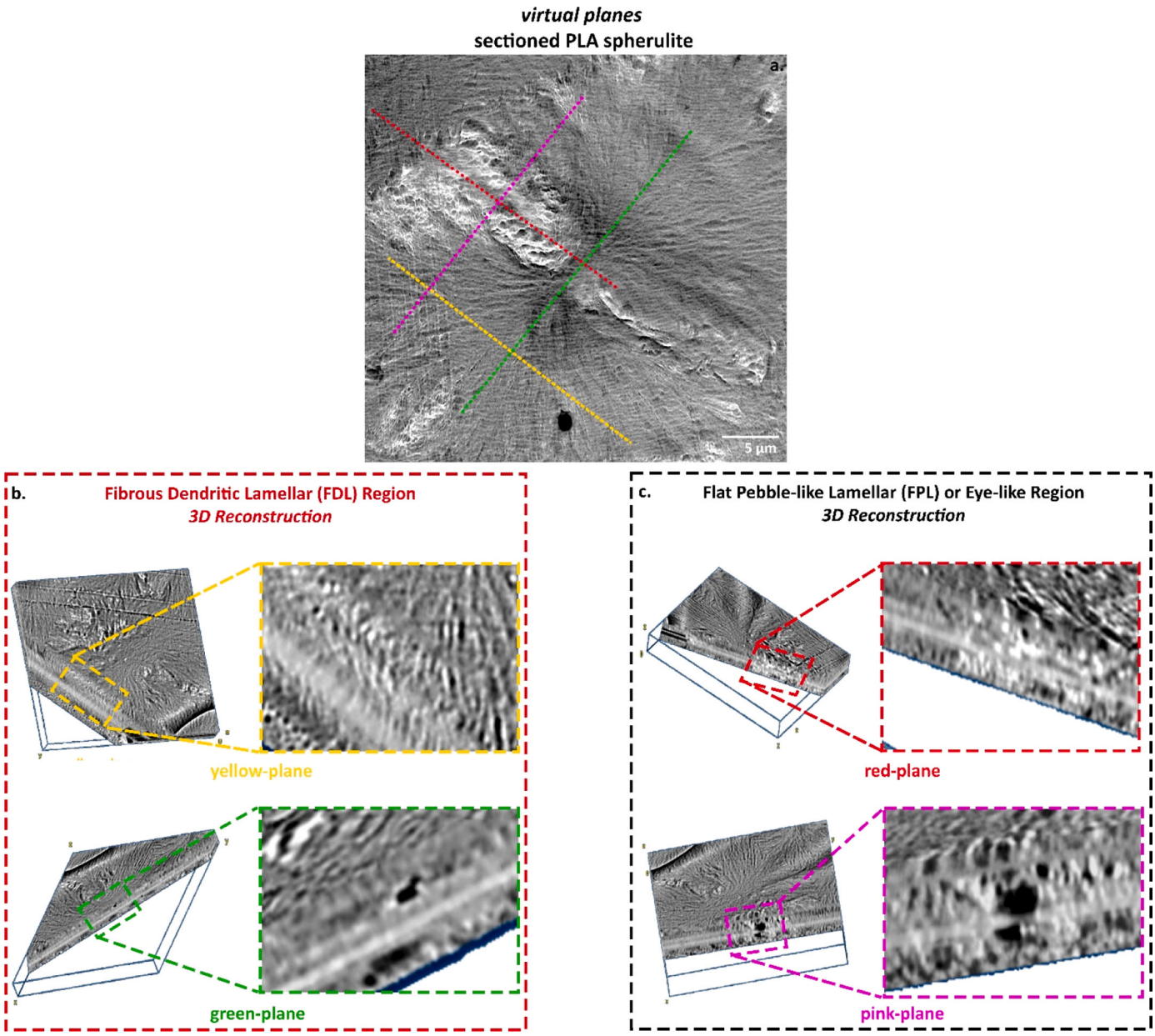

Fig. 10. Virtual cross sections of **a.** PLA spherulite and 3D volume reconstruction of its **b.** dendritic-lamellar (FDL) and **c.** pebble-like (FPL) regions.

lenghts, were found to be smaller (i.e., more elliptical shape) for the front and side-faces. This would be directly related to the development of shear flows, which originate at the mould walls. Shear flow causes deformation of the spherulites in one direction and a contraction in the exactly perpendicular one, known as Poisson's contraction [76]. Therefore, in the closest areas to the mould walls, the emergence of shear flow may have favoured the distortion of the spherulitic structures, promoting their elongation and, consequently, leading to an elliptical development, with respect to the inner-face ones.

In addition, the average spherulites area in the inner-face of the sample tends to be higher than what measured for the other two injection directions (Table 1.). The inner part of the specimen is less affected by the "thermal shock" owed to the passage of the polymer melt from the nozzle to the mould. Consequently, the temperature of the inner regions needs more time to settle down to the characteristic T_{mould}. This, therefore, exposes those areas to a longer residence time, at $T > T_{mould}$, which may promote the processes of crystallization and the spherulitic growth.

Lamellar development in spherulitic arrangements is barely studied for PLA, thus we decided to carry out an extensive characterization of the spherulite morphology at the inner-face, as shown in Fig. 9.

Polymer melt crystallization may result in a variety of spherulitic morphologies depending on the self-assembly tendencies of the polymer at a particular crystallization condition. For the PLA-based samples, spherulite has often described as only made up of fibrous/dendrite lamellae that develop and radiate outward from a shared nucleus centre [66,77]. Here, in contrast, the carried-out TEM imaging (Fig. 9.) suggests that the spherulite of PLA, isothermally crystallized at $T_{mould} = 110\ ^{\circ}C$, is divided into two mutually and perpendicularly oriented characteristic zones: an eye-like region that seem composed by flat pebble-like lamellae (FPL) and, the other one, consisting in fibrous dendritic ones (FDL), with tree-branch-like growth.

Along the direction of the sheaf-like nuclei, larger dendritic lamellae develop considerably more rapidly and occasionally bend and branch out as they expand outward, giving the appearance of highly dendritic region(s). These regions occupy a larger area than the FPL ones, with

sheaf-like arrangements whose ends are continuously branching and bending, multiplying into hundreds of crosshatched branches, and spreading out in a fan-like manner from the nucleation centre (Fig. 9b.). Their morphological development appears to be more pronounced for the lamellar structures (FDL) that grow and reach more peripheral areas than what occurs in the FPL region. Indeed, the pebble-like lamellae show a more limited extension in proximal areas to the nucleation centre.

On the other hands, the pebble-like structures originate from the same nucleation centre in an eye-like geometry region (FPL), whose boundaries are determined by surrounding sheaf-like lamellar zones (FDL). This eye-like region is filled with packed smooth texture-less structures, with pebble-like crystals appearing as flattened regions (Fig. 9c.), with different shapes.

Remarkably the structure of the spherulites observed in TEM images agrees perfectly with the four sectors optical images obtained by cross polarizers confirming that the effect on the light polarization plane is strictly correlated with the different orientation of the lamellae morphology, as revealed by TEM.

Generally, this type of spherulitic structure has been reported in materials crystallized in polymer diluents [78] and in PLA blends with PMMA [77] or PVPh [79], as a result of mutual and reciprocal interactions with the different components in the system.

The here investigated PLA is the single component of the system, characterized by a D-content lower than 1%. It is, therefore, possible to speculate that the presence of the stereoisomeric D-form may account for the evidence of what here detected (Fig. 9.) once this spherulitic morphology is compared with a PLA entirely composed of L-isomers units (dendritic spherulitic morphology) [80].

It has been found that the presence of even small percentages of D-isomeric units in the PLA chain during crystal structure formation leads to a reduction in the maximum achievable crystallinity and a slowing down of the crystallisation process [81]. As a result, the presence of the D-isomer is “perceived” by the PLA crystalline structure as a real defective element [82]. Indeed, recent studies have shown that the presence of D-isomers within PLA slightly distorts the conformation of the polymer chain helix due to a different intermolecular dipole-dipole interaction of the CH_3 group in PDLA systems compared to PLLA ones [83,84].

According to Tashiro et al. [85], the mutual interaction between the D and L units promotes the formation of more hydrogen bonds, which compact the structure by inhibiting the movement of the polar cloud of ester groups, forcing the chains into a “twisting distortion”. The folding of the polymer chain in the resulting lamellar arrangement would then be changed, leading to the same distortion. This, due to the relative movement of “interacting” lamellae during the crystalline growth, leads to an imbalance of surface stresses on the opposite surfaces of the lamellae, resulting in the phenomenon of twisting [86]. For instance, also during the crystallisation process of the chiral poly(epichlorohydrin), the presence of lamellar twisting has been observed [87]. Consequently, the conformational chirality of the chain helixes becomes an important parameter to be considered. Evidence of lamellar twisting is detected by TEM analysis from twist-like structures, precisely in the FPL regions of the spherulite (Fig. 9c. and Fig. 11c.).

From the TEM-imaging investigation, it appears clear that the spherulites have a complex three-dimensional arrangement of the PLA lamellae. Hence, by only attempting to reconstruct the entire spherulite volume it would be possible to understand their structures. For this purpose, serial sectioning experiments were performed. In serial sectioning, a sequence of consecutive ultrathin sections is collected and each of them is imaged. Each image is then aligned with the previous one and finally the entire volume is reconstructed by merging together them all by using the software ImageJ [88]. The entire procedure is depicted in Fig. 1**c.** for the serial sectioning of a spherulite belonging to the block inner-face. In this way, it is possible to visualize both the entire volume of the spherulite in a cumulative thickness of approx. 1.1 μm and

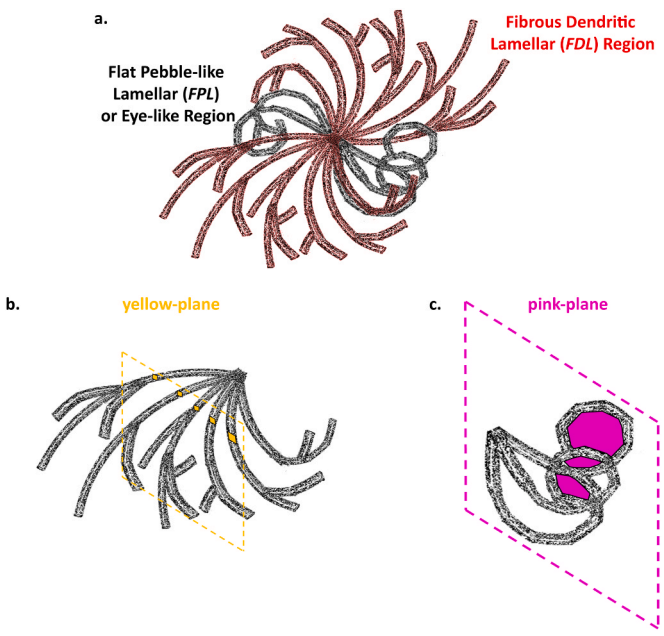

Fig. 11. a. Graphical schematizations of lamellar arrangements in FDL and FPL regions, with **b.** FDL and **c.** FPL regions visualization of the yellow and pink planes, according to what reconstructed thanks to the serial sectioning procedure.

its lamellar arrangements in the FDL and FPL regions (Fig. 10.).

Cross sections of the volume across the FDL dendritic region show ribbon-like organization of PLA lamellae (Fig. 10b. and Fig. 11b.). On the other hand, in the FPL region, the lamellae tend to twist, also becoming entangled with each other (Fig. 10c.). Consequently, depending on the inclination of the sectioning, the angle between the cutting plane and the lamellar structure will be different (Fig. 10d. and Fig. 11c.). Moreover, in some areas of the FPL region it is possible to detect the surfaces of elongated lamellae, like those found in the dendritic zone. Indeed, in that area those lamellae might be oriented exactly parallel to the cutting plane (Fig. 10c.).

4. Conclusions

Morphological studies provide important information about the characteristic structures of materials, such as degree of crystallinity (defects, disorder, crystallite size, etc.), crystalline orientation, surface texture analysis, grain size, specific surface area, porosity, density, etc. Moreover, poly-lactic acid (PLA) morphology is strictly related to its macroscopic properties. Thus, studying PLA ultrastructure represents an essential step toward the optimization of the industrial processing of this material, with the aim at producing PLA with characteristics that are tailored on its specific applications. Among the imaging techniques for studying polymer morphology, transmission electron microscopy (TEM) provides detailed information of the material ultrastructure.

Therefore, in this study, an extensive TEM characterization of the biobased and biodegradable PLA has been proposed. The optimization of sample preparation for improving TEM imaging was firstly shown; this aspect is particularly challenging when dealing with plastics (low image contrast, difficult sample preparation and radiation damage). Then, new insights concerning the structure of the injection-moulded PLA were obtained: 1) the characteristic spherulites structure description and of their three-dimensional arrangements; 2) the role and impact of D-isomer within the PLA material in determining the spherulitic development.

Thus, this work shed new light into the PLA morphology, laying the basis for future studies which aim to investigate how certain processing

parameters (polymeric melt flow orientation within the mould, moulding procedures, and different industrial conditions) exert a remarkable influence on polymer-based product morphology, which is directly related to its macroscopic properties such as strength, flexibility, transparency, and thermal behaviour.

CRediT authorship contribution statement

Aliotta Laura: Methodology, Supervision. **Parlanti Paola:** Conceptualization, Data curation, Investigation, Methodology, Validation, Writing – review & editing. **Lazzeri Andrea:** Conceptualization, Funding acquisition, Supervision, Writing – review & editing. **Molinari Giovanna:** Conceptualization, Data curation, Investigation, Methodology, Writing – original draft. **Gemmi Mauro:** Conceptualization, Funding acquisition, Supervision, Writing – review & editing.

Declaration of Competing Interest

The authors declare that they have no known competing financial interests or personal relationships that could have appeared to influence the work reported in this paper.

Data Availability

Data will be made available on request.

Acknowledgements

The authors acknowledge Prof. Luigi Folco (Dipartimento di Scienze della Terra, University of Pisa, Italy) for his assistance in the polarized light microscopy analysis.

References

[1] Polymers Used in Daily Life, StudiousGuy. https://studiousguy.com/polymers-used-in-daily-life/, 2010 (accessed 28 December 2023).StudiousGuy. Polymers Used in Daily Life.
[2] A.L. Andrady, M.A. Neal, Applications and societal benefits of plastics, Philos. Trans. R. Soc. B Biol. Sci. 364 (2009) 1977–1984.
[3] A. Costa, T. Encarnação, R. Tavares, T. Todo Bom, A. Mateus, Bioplastics: innovation for green transition, Polymers 15 (2023) 517.
[4] L.E. Haram, J.T. Carlton, G.M. Ruiz, N.A. Maximenko, A plasticene lexicon, Mar. Pollut. Bull. 150 (2020), 110714.
[5] National Academy of Science. Bio-based Industrial Products: Research and Commercialization Priorities. (2000).
[6] PLA: becoming a market leader in bioplastics, Total Corbion PLA formally starts up operations. https://www.european-bioplastics.org/total-corbion-pla-formally-starts-up-operations/, 2017. (accessed 27 December 2023).
[7] S. Sharma, Polylactic acid (PLA) and its composites: an eco-friendly solution for packaging, Sustain. Food Packag. Technol. (2021) 107–132, https://doi.org/10.1002/9783527820078.ch4.
[8] S. Farah, D.G. Anderson, R. Langer, Physical and mechanical properties of PLA, and their functions in widespread applications — a comprehensive review, Adv. Drug Deliv. Rev. 107 (2016) 367–392.
[9] J.L. Robert, K.B. Aubrecht, Green chemistry: ring-opening polymerization of lactide to form a biodegradable polymer, J. Chem. Educ. 85 (2008) 258–260.
[10] F. Gironi, V. Piemonte, Bioplastics and petroleum-based plastics: strengths and weaknesses, Energy Sources, Part A Recover. Util. Environ. Eff. 33 (2011) 1949–1959.
[11] C. Kourmentza, et al., Recent advances and challenges towards sustainable polyhydroxyalkanoate (PHA) production, Bioengineering 4 (2017) 1–43.
[12] M.A. Woodruff, D.W. Hutmacher, The return of a forgotten polymer - polycaprolactone in the 21st century, Prog. Polym. Sci. 35 (2010) 1217–1256.
[13] M. Jamshidian, E.A. Tehrany, M. Imran, M. Jacquot, S. Desobry, Poly-lactic acid: production, applications, nanocomposites, and release studies, Compr. Rev. Food Sci. Food Saf. 9 (2010) 552–571.
[14] E. Castro-Aguirre, F. Iñiguez-Franco, H. Samsudin, X. Fang, R. Auras, Poly(lactic acid)—mass production, processing, industrial applications, and end of life, Adv. Drug Deliv. Rev. 107 (2016) 333–366.
[15] Popelka, A., Zavahir, S., Habib, S. Morphology analysis. Polymer Science and Innovative Applications (INC, 2020). doi:10.1016/b978–0-12–816808-0.00002–0.
[16] H. Jinnai, R.J. Spontak, Transmission electron microtomography in polymer research, Polym. (Guildf.) 50 (2009) 1067–1087.
[17] M. Ilett, et al., Analysis of complex, beam-sensitive materials by transmission electron microscopy and associated techniques: TEM of beam sensitive materials, Philos. Trans. R. Soc. A Math. Phys. Eng. Sci. 378 (2020).
[18] S. Tencé-Girault, V. Woehling, E.K. Oikonomou, S. Karpati, S. Norvez, About the art and science of visualizing polymer morphology using transmission electron microscopy, Macromol. Chem. Phys. 219 (2018).
[19] B. Kuei, M.P. Aplan, J.H. Litofsky, E.D. Gomez, New opportunities in transmission electron microscopy of polymers, Mater. Sci. Eng. R. Rep. 139 (2020), 100516.
[20] Ayache, J., Beaunier, L., Boumendil, J., Ehret, G. Laub, D. Sample Preparation Handbook for Transmission Electron Microscopy. Sample Preparation Handbook for Transmission Electron Microscopy (2010). doi:10.1007/978–0-387–98182-6.
[21] J. Liu, X. Yu, L. Xue, Y. Han, Morphology Control of Polymer thin Films, in: *Polymer Morphology*, Wiley, 2016, pp. 299–316, https://doi.org/10.1002/9781118892756.ch16.QIPENG GUO. POLYMER MORPHOLOGY. News.Ge.
[22] Goerg H. Michler. Electron Microscopy of Polymers, First ed., Springer, Halle/Merseburg, 2008.
[23] A. Sionkowska, The processes induced by UV light in biopolymers and biopolymer composites, Mol. Cryst. Liq. Cryst. 590 (2014) 17–23.
[24] E.H. Arias-Nava, B.P. Sullivan, D.J. Valles-Rosales, Biopolymer degradation analysis: accelerated life testing study to characterize polylactic acid durability, Materials 14 (2021) 1–13.
[25] B. Kuei, E.D. Gomez, Pushing the limits of high-resolution polymer microscopy using antioxidants, Nat. Commun. (12, () (2021).
[26] J.R. Ebdon, T.N. Huckerby, I. Khan, An improved permanganic etchant for polyolefines, Polym. Commun. (Guildf., Engl.) 24 (1983) 162–165.
[27] Cubri, G. & Kati, I. Evaluation of Changes in Polymer Material Properties Due to Aging in Different Environments. (2022).
[28] E. Nogales, S.H.W. Scheres, Cryo-EM: a unique tool for the visualization of macromolecular complexity, Mol. Cell 58 (2015) 677–689.
[29] A. Al-Amoudi, J. Dubochet, H. Gnaegi, W. Lüthi, D. Studer, An oscillating cryo-knife reduces cutting-induced deformation of vitreous ultrathin sections, J. Microsc. 212 (2003) 26–33.
[30] B. Kuei, M.P. Aplan, J.H. Litofsky, E.D. Gomez, New opportunities in transmission electron microscopy of polymers, Mater. Sci. Eng. R. Rep. 139 (2020), 100516.
[31] P. Doshev, et al., Phase interactions and structure evolution of heterophasic ethylene-propylene copolymers as a function of system composition, J. Appl. Polym. Sci. 101 (2006) 2825–2837.
[32] Physics, T. & Bar, S. Ruthenium Tetraoxide Staining of Polymers:New Preparative Methods for Electron Microscopy. 2930–2931 (1984).
[33] Injection moulding for plastics processing, fisem. https://www.fisem.it/en/injection-molding/ (accessed 27 December 2023).fisem. Injection moulding for plastics processing.
[34] C. Ye, et al., Rapid assessment of crystal orientation in semi-crystalline polymer films using rotational zone annealing and impact of orientation on mechanical properties, Soft Matter 13 (2017) 7074–7084.
[35] T. Feng, et al., Size effects in the thermal conductivity of amorphous polymers, Phys. Rev. Appl. 14 (2020) 1.
[36] N.P. Bessonova, S.V. Krasheninnikov, M.A. Shcherbina, S.N. Chvalun, Thermal behavior of crystalline and amorphous HDPE phase in the process of necking at creep deformation, Polym. Test. 97 (2021), 107127.
[37] U.K. Murmu, et al., Mechanical properties of crystalline and semicrystalline polymer systems, Encycl. Mater. Plast. Polym. 1–4 (2022) 917–927.
[38] M. Kaszonyiova, F. Rybnikar, J. Sadilek, J. Kucera, M. Kubisova, Oriented isotactic polypropylene structure and morphology, IOP Conf. Ser. Mater. Sci. Eng. (448) (2018).
[39] Y. Lin, E. Bilotti, C.W.M. Bastiaansen, T. Peijs, Transparent semi-crystalline polymeric materials and their nanocomposites: a review, Polym. Eng. Sci. 60 (2020) 2351–2376.
[40] Can PLA plastic be injection molded?, ZETARMOLD. https://zetarmold.com/pla-plastic-be-injection-molded/#:~:text=PLAhasgoodthermalstability,as%20extrusion%2Candinjectionmolding, 2022 (accessed 28 December 2023).
[41] S. Körber, K. Moser, J. Diemert, Development of high temperature resistant stereocomplex PLA for injection moulding, Polymers 14 (2022).
[42] L. Wang, W.M. Gramlich, D.J. Gardner, Improving the impact strength of Poly (lactic acid) (PLA) in fused layer modeling (FLM), Polymers 114 (2017) 242–248.
[43] L. Aliotta, L.M. Sciara, P. Cinelli, I. Canesi, A. Lazzeri, Improvement of the PLA crystallinity and heat distortion temperature optimizing the content of nucleating agents and the injection molding cycle time, Polymers 14 (2022) 977.
[44] S. Jia, et al., Morphology, crystallization and thermal behaviors of PLA-based composites: wonderful effects of hybrid GO/PEG via dynamic impregnating, Polymers 9 (2017).
[45] C. Fosse, et al., Determination of the equilibrium enthalpy of melting of two-phase semi-crystalline polymers by fast scanning calorimetry, Thermochim. Acta 677 (2019) 67–78.
[46] R.C. Zhang, et al., Equilibrium melting temperature of polymorphic poly(L-lactide) and its supercooling dependence on growth kinetics, Polymers 9 (2017).
[47] E.W. Fischer, H.J. Sterzel, G. Wegner, Investigation of the structure of solution grown crystals of lactide copolymers by means of chemical reactions, Kolloid-Z. Z. für Polym. 251 (1973) 980–990.
[48] A. Moscardini, et al., Uranium-free X solution: a new generation contrast agent for biological samples ultrastructure, Sci. Rep. 10 (2020) 1–11.
[49] O. Mysiukiewicz, M. Barczewski, K. Skórczewska, D. Matykiewicz, Correlation between processing parameters and degradation of different polylactide grades during twin-screw extrusion, Polymers 12 (2020).
[50] R.A. Chivers, D.R. Moore, The effect of molecular weight and crystallinity on the mechanical properties of injection moulded poly(aryl-ether-ether-ketone) resin, Polymers 35 (1994) 110–116.

[51] Y. He, D. Liu, J. Wang, P. Pan, W. Hu, Tammann analysis of the molecular weight selection of polymorphic crystal nucleation in symmetric racemic Poly(lactic acid) blends, Macromolecules (2022), https://doi.org/10.1021/acs.macromol.2c00457.
[52] L. Meinig, R. Boldt, Y. Spoerer, I. Kuehnert, M. Stommel, Correlation between processing parameters, morphology, and properties of injection-molded polylactid acid (PLA) specimens at different length scales, Polymers 15 (2023).
[53] M. Yasuniwa, S. Tsubakihara, Y. Sugimoto, C. Nakafuku, Thermal analysis of the double-melting behavior of poly(L-lactic, Acid.). *J. Polym. Sci. Part B Polym. Phys.* 42 (2004) 25–32.
[54] Y. Xu, H.B. Jia, S.R. Ye, J. Huang, Effect of melting conditions on crystallization behavior of poly(trimethylene terephthalate), E-Polym. (2008) 1–7, https://doi.org/10.1515/epoly.2008.8.1.58.
[55] C.A. Gracia-Fernández, S. Gómez-Barreiro, J. López-Beceiro, S. Naya, R. Artiaga, New approach to the double melting peak of poly(l-lactic acid) observed by DSC, J. Mater. Res. 27 (2012) 1379–1382.
[56] Lorenzo, M.L. Di & Androsch, R. Synthesis, Structure and Properties of Poly(lactic acid). (Springer US).
[57] T. Farid, V.N. Herrera, O. Kristiina, Investigation of crystalline structure of plasticized poly (lactic acid)/Banana nanofibers composites, IOP Conf. Ser. Mater. Sci. Eng. 369 (2018).
[58] Polymers in Polarized Light, Phillip C., Robinson, M.W.D. https://micro.magnet.fsu.edu/primer/techniques/polarized/polymers.html, 1998-2002 (accessed 28 December 2023).
[59] A.M. El-Hadi, Increase the elongation at break of poly (lactic acid) composites for use in food packaging films, Sci. Rep. 7 (2017).
[60] J. Xu, H. Ye, S. Zhang, B. Guo, Organization of twisting lamellar crystals in birefringent banded polymer spherulites: a mini-review, Crystals 7 (2017).
[61] Woo, E.M. *et al.* Surface and interior views on origins of two types of banded spherulites. (2021) doi:10.1002/pen.21991.
[62] L. Gránásy, T. Pusztai, J.F. Douglas, Insights into polymer crystallization from phase-field theory, Encycl. Polym. Compos. (2013), https://doi.org/10.1007/978-3-642-37179-0_30-1.
[63] M. Safandowska, A. Rozanski, A. Galeski, Plasticization of polylactide after solidification: an effectiveness and utilization for correct interpretation of thermal properties, Polymers 12 (2020).
[64] M. Safandowska, A. Rozanski, Ring-banded spherulites in polylactide and its blends, Polym. Test. 100 (2021), 107230.
[65] N. Haque, R.F. Cochrane, A.M. Mullis, Morphology of spherulites in rapidly solidified Ni3Ge droplets, Crystals 7 (2017) 1–12.
[66] G. Lugito, E.M. Woo, Asymmetric growth of co-crystallized nano-and micrometer-sized lamellae to Janus-faced spherulites in poly(L-lactic acid) with amorphous poly(methyl methacrylate), Cryst. Growth Des. 17 (2017) 5034–5037.
[67] M.A. Elsawy, K.H. Kim, J.W. Park, A. Deep, Hydrolytic degradation of polylactic acid (PLA) and its composites, Renew. Sustain. Energy Rev. 79 (2017) 1346–1352.
[68] A. Szucs, K. Belina, Rheological and thermal analysis of the filling stage of injection moulding, Express Polym. Lett. 6 (2012) 672–679.
[69] B. Cai, et al., Structural characterization of oligosaccharide from Spirulina platensis and its effect on the faecal microbiota in vitro, Food Sci. Hum. Wellness 11 (2022) 109–118.
[70] C. Ye, et al., Rapid assessment of crystal orientation in semi-crystalline polymer films using rotational zone annealing and impact of orientation on mechanical properties, Soft Matter 13 (2017) 7074–7084.
[71] Bayer, R.K., Zachmann, H.G. Kassel, G. Pol yet h ylene. Part 1: Influence of Mold Geometry. 29, (2000).
[72] R. Arrigo, G. Malucelli, F.P. Mantia, La. Effect of the elongational flow on the morphology and properties of polymer systems: a brief review, Polymers 13 (2021) 1–35.
[73] X. Chen, et al., Effect of molecular weight on crystallization, melting behavior and morphology of poly(trimethylene terephalate), Polym. Test. 26 (2007) 144–153.
[74] Erukhimovich, I. & de la Cruz, M.O. Phase equilibria and charge fractionation in polydisperse polyelectrolyte solutions. **48**, 1223–1234 (2004).
[75] R.K. Bayer, et al., Properties of elongational flow injection moulded polyethylene, J. Mater. Sci. 24 (1989) 2643–2652.
[76] P.H. Mott, C.M. Roland, Limits to Poisson's ratio in isotropic materials, Phys. Rev. B - Condens. Matter Mater. Phys. 80 (2009) 1–4.
[77] S. Nurkhamidah, E.M. Woo, Effects of stereocomplex nuclei or spherulites on crystalline morphology and crack behavior of poly(L -lactic acid), Macromol. Chem. Phys. 212 (2011) 1663–1670.
[78] G. Lugito, S. Nagarajan, E.M. Woo, Explosive Fibonacci-sequence growth into unusual sector-face morphology in poly(l-lactic acid) crystallized with polymeric diluents, Sci. Rep. 10 (2020) 1–14.
[79] S. Nurkhamidah, E.M. Woo, Mechanisms of multiple types of lamellae and spherulites in poly(l -lactic acid) interacting with poly(4-vinyl phenol), Macromol. Chem. Phys. 214 (2013) 2345–2354.
[80] S. Nurkhamidah, E.M. Woo, Y.T. Yeh, F. Luo, V. Katiyar, Lamellae assembly in dendritic Spherulites of Poly(L-lactic Acid) crystallized with poly(p-Vinyl Phenol), Polymers 10 (2018) 1–21.
[81] M.L. Di Lorenzo, R. Androsch, Influence of α′-/α-crystal polymorphism on properties of poly(l-lactic acid), Polym. Int. 68 (2019) 320–334.
[82] M.R. Mohamed Zin, A. Mahendrasingam, C. Konkel, T. Narayanan, Effect of D-isomer content on strain-induced crystallization behaviour of Poly(lactic acid) polymer under high speed uniaxial drawing, Polymers 216 (2021), 123422.
[83] H. Tsuji, Poly(lactide) stereocomplexes: Formation, structure, properties, degradation, and applications, Macromol. Biosci. 5 (2005) 569–597.
[84] D. Brizzolara, H.J. Cantow, R. Mülhaupt, A.J. Domb, Novel materials through stereocomplexation, J. Comput. Mater. Des. 3 (1996) 341–350.
[85] K. Tashiro, N. Kouno, H. Wang, H. Tsuji, Crystal structure of Poly(lactic acid) stereocomplex: random packing model of PDLA and PLLA chains as studied by X-ray diffraction analysis, Macromolecules 50 (2017) 8048–8065.
[86] D. Maillard, R.E. Prud'homme, Crystallization of ultrathin films of polylactides: From chain chirality to lamella curvature and twisting, Macromolecules 41 (2008) 1705–1712.
[87] Lorenzo, M.L., Di, Editors, R.A. Crystals and Crystallinity in Polymers. Crystals and Crystallinity in Polymers (2013). doi:10.1002/9781118690444.
[88] C. MessaoudiI, T. Boudier, C.O.S. Sorzano, S. Marco, TomoJ: Tomography software for three-dimensional reconstruction in transmission electron microscopy, BMC Bioinforma. 8 (2007).